A nanoplasmonic molecular ruler for measuring nuclease activity and DNA footprinting

GANG L. LIU[1], YADONG YIN[2,3‡], SIRI KUNCHAKARRA[2], BIPASHA MUKHERJEE[2], DANIELE GERION[2,4], STEPHEN D. JETT[5], DAVID G. BEAR[5], JOE W. GRAY[2], A. PAUL ALIVISATOS[2,3], LUKE P. LEE[1]* AND FANQING FRANK CHEN[2]*

[1]Biomolecular Nanotechnology Center, Department of Bioengineering, University of California at Berkeley, Berkeley, California 94720, USA
[2]Lawrence Berkeley National Laboratory, Berkeley, California 94720, USA
[3]Department of Chemistry, University of California, Berkeley, California 94720, USA
[4]Lawrence Livermore National Laboratory, Livermore, California 94551, USA
[5]Department of Cell Biology and Physiology and the Cancer Research and Treatment Center, University of New Mexico Health Sciences Center, Albuquerque, New Mexico 87131, USA
‡Present address: Department of Chemistry, University of California at Riverside, Riverside, California 92521, USA
*e-mail: lplee@berkeley.edu and f_chen@lbl.gov

Published online: 4 October 2006; doi:10.1038/nnano.2006.51

Interactions between nucleic acids and proteins are essential to genetic information processing. The detection of size changes in nucleic acids is the key to mapping such interactions, and usually requires substrates with fluorescent, electrochemical or radioactive labels[1–3]. Recently, methods have been developed to tether DNA to highly water-soluble Au nanoparticles[4–8], and nanoparticle pairs linked by DNA have been used to measure nanoscale distances[9]. Here we demonstrate a molecular ruler in which double-stranded DNA is attached to a Au nanoparticle. The change in plasmon resonance wavelength of individual Au–DNA conjugates depends on the length of the DNA and can be measured with subnanometre axial resolution. An average wavelength shift of approximately 1.24 nm is observed per DNA base pair. This system allows for a label-free, quantitative, real-time measurement of nuclease activity and also serves as a new DNA footprinting platform, which can accurately detect and map the specific binding of a protein to DNA.

Surface plasmon resonance (SPR) spectroscopy measures the refractive index or dielectric constant of liquids or media in contact with the surface of metallic thin films. Conventional bulk-scale SPR can measure analyte concentration, protein–protein interaction and DNA hybridization[10,11]. Recently, high-speed nanoplasmonic resonance sensing on a single metallic nanoparticle has been developed, and various methods have been reported for immobilizing biomolecules on metallic nanoparticles[12–20]. The plasmon resonance wavelengths of the Au nanoparticles shift in response to changes in their immediate environment, and the shift can be detected using scattering or absorption spectroscopy.

Here we designed a nanoplasmonic molecular ruler, with a 54-bp double-stranded DNA (dsDNA) as the enzymatic substrate and calibration standard, conjugated to a 20-nm Au nanoparticle (Figs 1 and 2). The dsDNA contained cleavage sites for the endonucleases *Hin*dIII, *Xho*I, *Sal*I and *Kpn*I, centred at nucleotide

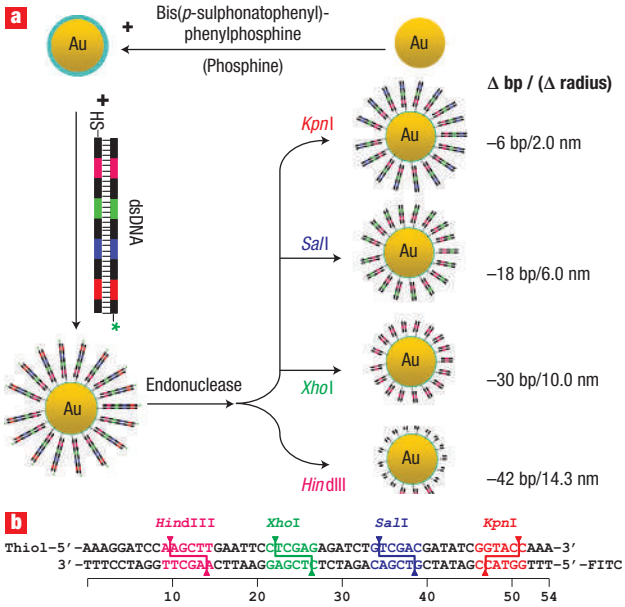

Figure 1 Design of the Au–DNA nanoplasmonic molecular ruler. a, Synthesis process of the Au–DNA nanoconjugate. The 20-nm Au nanoparticle modified with a phosphine surfactant monolayer was enclosed by a layer of synthesized 54-bp dsDNA. A thiol group and the FITC (fluorescein isothiocyanate) fluorophore (as indicated by green star) were synthesized at each end of the dsDNA, respectively. Through the thiol–Au chemistry, the dsDNA was tethered onto the Au nanoparticles. **b**, The dsDNA contains endonuclease incision sites positioned at 12, 24, 36 and 48 bp from the Au-nanoparticle-tethered end. The fluorescent labelling (FITC) is only for further confirmation of the nuclease reactions, and is not necessary for plasmon resonance measurements.

©2006 Nature Publishing Group

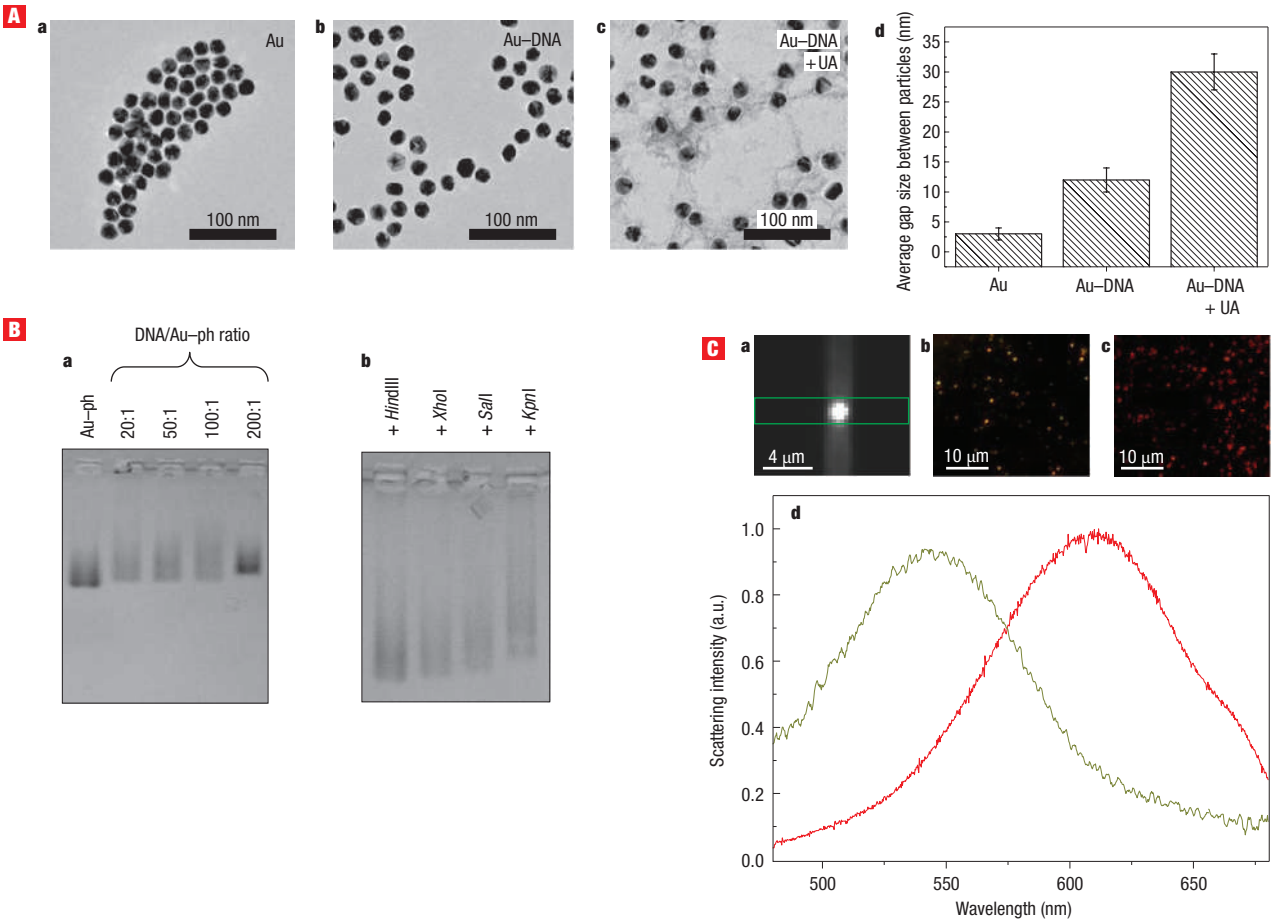

Figure 2 DNA conjugation red-shifted plasmon resonance peak of the molecular ruler. A, TEM images of nanoconjugates: **a**, Au; **b**, Au–DNA; **c**, Au–DNA with DNA stained by uranyl acetate (UA), which further increased the diameter of the complex (uneven DNA density is due to fixation); **d**, distances between the Au nanoparticles. The error bars represent the standard deviation in the measurement of 50 nanoparticles. **B**, Electrophoresis of nanoconjugates: **a**, Au–DNA nanoconjugates (Au–ph is phosphine-coated Au nanoparticle); **b**, Au–DNA nanoconjugates cleaved by four endonucleases, which led to the loss of 42, 30, 18 and 6 bps from the dsDNA, showing DNA size-dependent mobility. **C**, Dark-field scattering images: **a**, a single nanoparticle targeted and isolated from a field of Au–DNA nanoparticles for spectroscopic examination; **b**, **c**, true-colour images of Au (**b**) (540 nm peak) and Au–DNA (**c**) (607 nm peak); **d**, scattering spectra of Au (green line) and Au–DNA (red line).

positions 12, 24, 36 and 48, respectively. The surface density of dsDNA on the Au nanoparticles was controlled by their concentration ratio during immobilization. A 100:1 DNA/Au ratio was found to be the best compromise to preserve the natural extension of dsDNA (Fig. 2A), while allowing accessibility to the nuclease[21] (Fig. 2B). The surface modification of Au nanoparticles with dsDNA was confirmed by transmission electron microscopy (TEM) (Fig. 2A) and electrophoresis (Fig. 2B, a).

The scattering images and spectra of individual nanoconjugates were acquired using a dark-field microscopy system with a true-colour imaging charge-coupled device (CCD) camera and a spectrometer (Fig. 2C, a). Interestingly, Au (Fig. 2C, b), which carries no DNA but a phosphine surfactant (see Supplementary Information, Fig. S2), and Au–DNA (Fig. 2C, c) exhibit different colours in yellow and red, respectively. The attachment of DNA seems to red-shift the peak plasmon resonance wavelength of the Au nanoparticle by 67 nm (Fig. 2C, d). The ruler provides a new means for studying the kinetics of the nuclease enzymatic reactions. Real-time measurement of endonuclease activity and kinetics for one model endonuclease, *Xho*I, was demonstrated, and the average plasmon resonance wavelength drops after the *Xho*I endonuclease reactions due to the loss of 30 bp of dsDNA (Fig. 3; also see Supplementary Information, Fig. S3). EDTA-induced inhibition of *Xho*I reaction can also be visualized (Fig. 3B). The salt concentration change was negligible, as all components were preincubated with the same reaction buffer (Fig. 3B).

We then focused on the size effect of the attached DNA. In order to investigate whether the nanoplasmonic resonance frequency shift of the Au–DNA nanoconjugate can accurately reflect DNA size change, we artificially produced DNA size standards by endonuclease cleavage. About ten nanoconjugates from each sample were examined spectroscopically in dark field and the average plasmon resonance wavelengths are shown in Fig. 4. Au–DNA nanoconjugates were reacted with *Kpn*I, *Sal*I, *Xho*I and *Hin*dIII, which cleaved the first 6, 18, 30 and 42 bp from the distal end of the full-length dsDNA, respectively. Figure 4a shows the typical scattering spectra and plasmon resonance wavelengths of Au–DNA nanoconjugates after the 1-hour cleavage reactions. Figure 4b shows the plasmon resonance spectra of single Au nanoparticles tethered with 0, 12, 24, 36, 48 and 54 bp of dsDNA. The average wavelength blue shifts from the

©2006 Nature Publishing Group

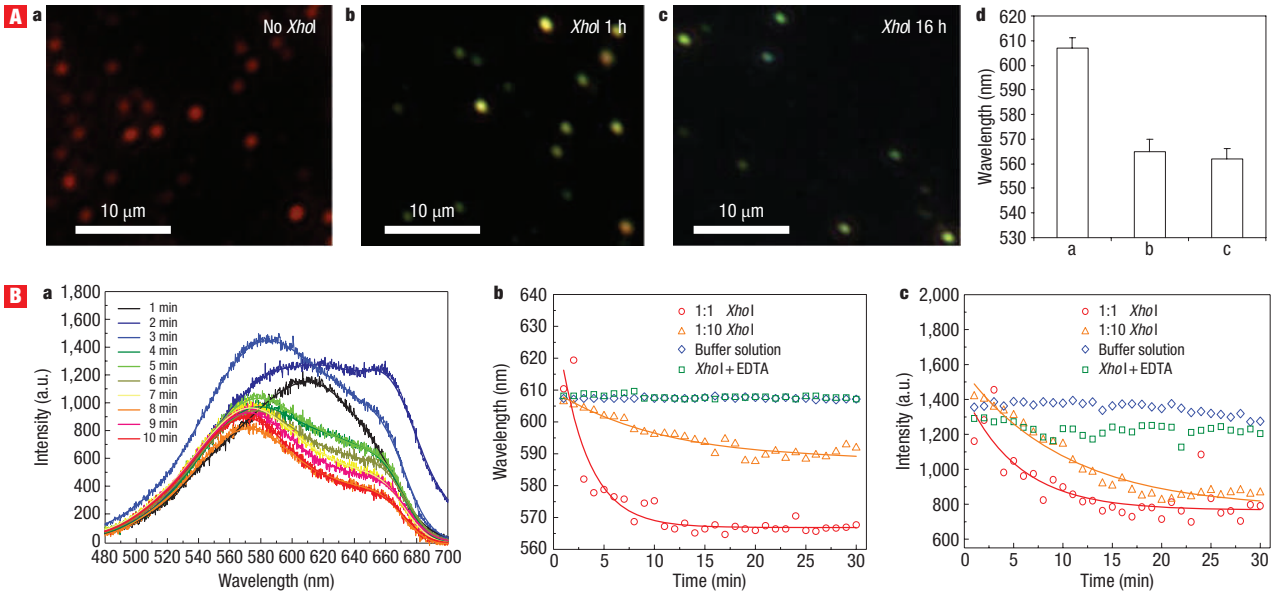

Figure 3 Endonuclease activity measurement with ruler. A, Plasmon resonance sensing with multiple nanoconjugates: **a–c**, dark-field scattering images of the Au–DNA nanoconjugates cleaved by endonuclease *Xho*I (**a**, before cleavage; **b**, 1 hour reaction with more than 90% cleavage; **c**, 16 hours reaction with 100% cleavage. See also Supplementary Information, Fig. S3 for validated cleavage); **d**, plasmon resonance wavelengths of the single Au nanoconjugates in **A**, **a–c**. The error bars represent the standard deviation in the measurement of 20 nanoparticles. **B**, Real-time plasmon resonance sensing of endonuclease reactions: **a**, raw scattering spectra data of a single Au–DNA nanoconjugate in an endonuclease reaction, time-resolved; **b**, plasmon resonance peak wavelength; **c**, scattering peak intensity of the Au–DNA nanoconjugate in the 30-min reactions with 1:1 *Xho*I (3.5 nM, red circles), 1:10 *Xho*I (350 pM, orange triangles), control buffer only (blue diamonds) and inhibitor/chelator EDTA (green squares). The plasmon resonance wavelength data exhibit a first-order exponential decay (red and orange curves).

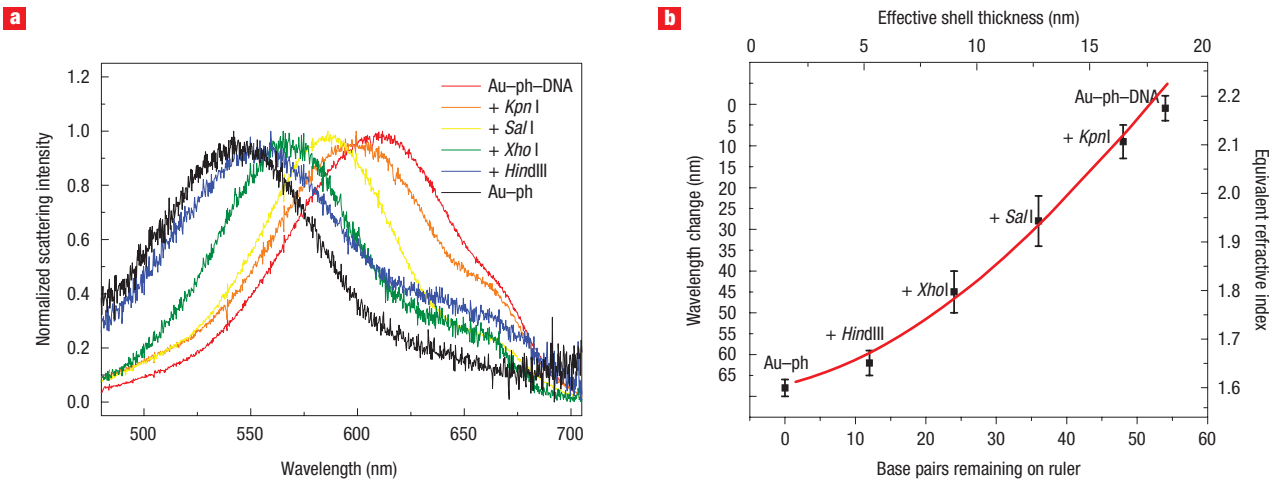

Figure 4 Calibration curve generated by nanoplasmon resonance sensing of multiple enzymes. a, Typical scattering spectra. **b**, Plasmon resonance peak wavelengths of the Au–DNA nanoconjugates after cleavage reactions with four endonuclease enzymes, and as a function of the number of base pairs remaining attached to the Au nanoparticle after the cleavage. The red curve is a fit from a semi-empirical model using a Langevin-type dependence of the refractive index versus dsDNA length (see Supplementary Information, Fig. S4 and Table S1). The error bars represent the standard deviation in the measurement of 20 nanoparticles.

Au–DNA were approximately 67 nm, 62 nm, 45 nm, 28 nm, 10 nm and 0 nm, respectively. The plasmon resonance shift of the nanoparticle corresponded to the change of the dielectric layer around the nanoparticle and is related to the length of the digested dsDNA. Using the Mie scattering calculation for coated Au nanoparticles[22], the equivalent dielectric constant, or refractive index of the biopolymer shell (dsDNA + phosphine), was obtained (Fig. 4b; see Supplementary Information, Table S1 and Fig. S4). The relationship between the dsDNA length and the equivalent refractive index showed a good agreement with the quadratic Langevin model[23] (red fitted curve in Fig. 4b; see Supplementary Information). An average wavelength shift of $\sim$1.24 nm bp^{-1} was observed. Note that the full length of the complete dsDNA ($\sim$20 nm) is much longer than the effective

©2006 Nature Publishing Group

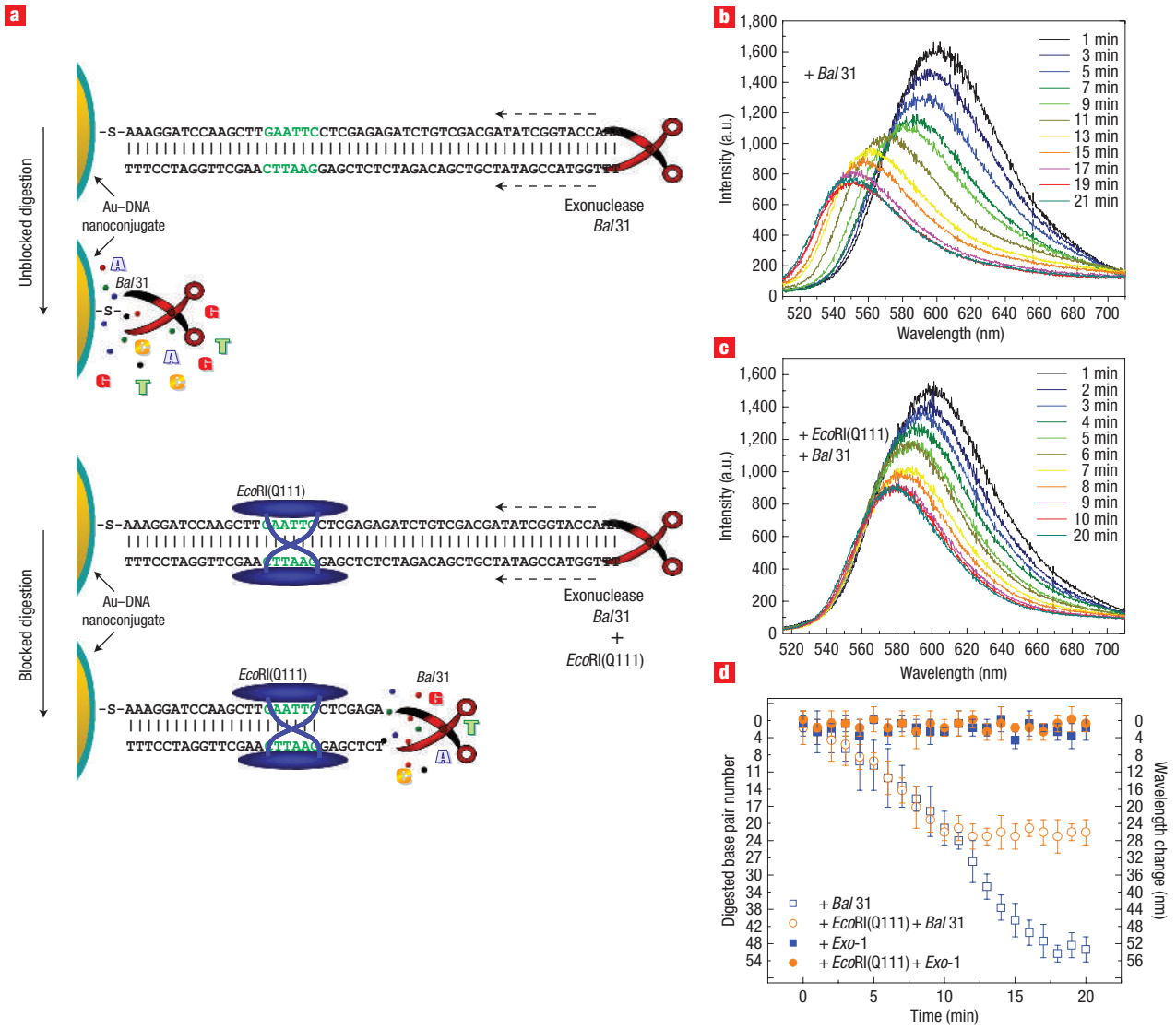

Figure 5 DNA footprinting of *Bal*31 exonuclease stalled by the *Eco*RI(Q111) proteins. a, Schematic diagram of footprinting by *Bal*31 and the stalled *Bal*31 hydrolysis by DNA-bound *Eco*RI(Q111) protein. The *Eco*RI(Q111) blocks nucleotide removal by *Bal*31 on a single Au–DNA nanoconjugate. **b**,**c**, Time-lapse scattering spectra of the single Au–DNA nanoconjugates without *Eco*RI(Q111) (**b**) and with *Eco*RI(Q111) (**c**) during exonuclease *Bal*31 hydrolysis. **d**, Plasmon resonance wavelength of the Au–DNA nanoconjugate as a function of time in the exonuclease reactions, with wavelength shift shown on the right vertical axis and the base pair of the dsDNA removed on the left vertical axis. The error bars represent the standard deviation in the measurement of 10 nanoparticles.

Förster transfer distance (<10 nm), so the ruler has a longer detection range than the Förster resonance energy transfer.

Based on the established correlation curve between the shifts in the plasmon wavelength and the DNA size (Fig. 4b), DNA length in a nuclease reaction can be determined, which allows us to measure the footprint of DNA-binding proteins. *Eco*RI(Q111) protein was used as a model protein in exonuclease-based DNA footprinting. *Eco*RI(Q111) is a cleavage-defective variant of the *Eco*RI protein with amino acid residue 111 mutated to glutamine (Q). *Eco*RI(Q111) still maintains specific binding activity to the sequence GAATTC on dsDNA, but does not cleave DNA[24,25]. *Eco*RI(Q111) has previously been used to block a transcription elongation complex[26]. As depicted in Fig. 5a, *Eco*RI(Q111) binds to the GAATTC sequence on the Au–DNA nanoconjugates. Subsequently an exonuclease enzyme, *Bal*31, is introduced to degrade the dsDNA from the untethered end without any specificity. *Bal*31 exonuclease degrades both 3′ and 5′ termini of dsDNA[27]. Fig. 5b,c shows the scattering spectra of the Au–DNA nanoconjugate digested by *Bal*31, without and with the bound *Eco*RI(Q111), respectively. For the unbound DNA, the plasmon resonance wavelength of the nanoconjugate was blue-shifted ~52 nm by *Bal*31 in 20 min and stabilized afterwards (blue squares, Fig. 5d); however, for the DNA bound by the *Eco*RI(Q111), the plasmon resonance wavelength of the nanoconjugate shifted a maximum of 25 nm before stabilization (red circles, Fig. 5d). The corresponding base pair length of the degraded dsDNA was calculated according to the fitted quadratic Langevin model (see Supplementary Information). The *Bal*31 exonuclease digested almost all (~90%) of the 54 bp of the dsDNA, but it digested only ~25 bp with the *Eco*RI(Q111) blocking procession of *Bal*31 exonuclease. The stalling point of the exonuclease is around 25 ± 3 bp from the distal end of the

©2006 Nature Publishing Group

DNA, which is approximately 7 bp from the GAATTC site, and is in perfect agreement with previous measurements using conventional radiolabels (7 ± 3 bp)[25]. Previous mapping indicates that *Eco*RI(Q111) binds to 3 bp of dsDNA flanking the 3′ boundary of the GAATTC sequence, and the steric exclusion between *Eco*RI(Q111) and exonuclease contributes to the other 4 bp. A control exonuclease, *Exo*-1, which does not cleave dsDNA, showed no effect on the ruler spectra (Fig. 5d).

The magnitudes of plasmon resonance shifts in our experiments are greater than previous reports on other biochemical reactions such as protein binding. We attribute the relatively larger wavelength shift to the stiffness of dsDNA axially and the unique dependence of its dielectric constant on its length. Additionally, the proteins and DNA have distinct electron densities, and it seems that the DNA scattering potential is one order of magnitude higher than that of the proteins. Therefore, the partial shortening or extension of the dsDNA will lead to a proportionally larger change around the Au surface compared with the change induced by a coiled protein binding or disassociation event. Furthermore, the DNA length shortening is also accompanied by a considerable decrease of DNA refractive index (see Supplementary Information, Table S1). An independent study by Doron-Mor and colleagues showed coordination-based self-assembled multilayers can offer thickness tuning of Au nanoparticle SPR spectra in the range 1–15 nm[28,29], further validating our observation that nanoplasmonic spectra shift can be correlated with DNA length. The irregularity in the size and shape of the Au nanoparticles is possibly a contributing factor in the broadening of the spectra, and the resulting standard deviation. The accuracy and spectral resolution of our measurements can be further improved by using nanoparticles with better shape and size controls.

The time resolution of the nanoplasmonic molecular ruler can be as high as one spectrum per second by taking advantage of the high quantum efficiency of Rayleigh scattering compared with fluorescence or Raman scattering; therefore biomolecular reactions in the timescale of seconds can also be measured. Although only a simple dsDNA substrate is used here, there is no limitation to the sequences or structure of the oligonucleotide substrates. The ability to resolve a single nanoparticle without the need for radioactive or fluorescent labelling also makes it possible to perform high-throughput screening in a high-density microarray or in microfluidic devices. The technology can also be used for the detection of other enzymes that induce length changes.

METHODS

PREPARATION OF THE dsDNA-CONJUGATED Au NANOPARTICLE

The dsDNA (Fig. 1b; see Supplementary Information) was mixed with the concentrated phosphine-coated Au nanoparticles (see Supplementary Information, Fig. S2) in a molar ratio of 200:1, 100:1, 50:1 and 20:1, at room temperature for about 12 h, then stored at −20 °C. Electrophoresis was used to verify the DNA attachment (Fig. 2B, a). The decreased mobility of the DNA-conjugated gold particles was clearly observed, indicating the successful DNA attachment to the gold nanoparticles. The presence of DNA can be confirmed by TEM imaging, with or without uranyl acetate staining (provided by Mark Le Gros), and the extra stain further increased the effective diameter of the whole complex (Fig. 2A).

SCATTERING IMAGING AND SPECTROSCOPY OF SINGLE Au–DNA NANOCONJUGATES

The microscopy system consisted of a Carl Zeiss Axiovert 200 inverted microscope (Carl Zeiss) equipped with a dark-field condenser ($1.2 <$ (numerical aperture) < 1.4), a true-colour digital camera (CoolSNAP*cf*, Roper Scientific) and a 300 mm focal length and 300 grooves per mm monochromator (Acton Research) with a 1024×256 pixel cooled spectrograph CCD camera (Roper Scientific). A 2-μm-wide aperture was placed in front of the entrance slit of the monochromator to keep only a single nanoparticle in the region of interest. After photobleaching the fluorescence, the true-colour scattering images of Au–DNA nanoconjugates were taken using a ×60 objective lens (numerical aperture = 0.8) and the true-colour camera with a white light illumination from a 100 W halogen lamp. The scattering spectra of Au–DNA nanoconjugates were routed to the monochromator and spectrograph CCD. Raw spectra were normalized with respect to the spectrum of a nonresonant nanoparticle (polystyrene) after background subtraction. In the real-time spectroscopy experiments, the nanoparticle-immobilized glass slide was mounted on a transparent indium tin oxide (ITO) heater with an external thermostat and heated to 37 °C or 25 °C. The immobilized nanoparticles were immersed in a drop of buffer solution, which also served as the contact fluid for the dark-field condenser. The endonuclease or exonuclease enzymes with buffer solution were loaded by pipette into the contact fluid and the continuous spectrum acquisition started simultaneously. The microscopy system was completely covered by a dark shield, which prevented ambient light interference and excessive evaporation.

CLEAVAGE REACTION OF dsDNA ON Au–DNA NANOPARTICLE CONJUGATE

We immobilized the Au–DNA nanoconjugates electrostatically on an ultraclean thin glass slide. The cleavage reaction for DNA was performed with endonucleases *Hin*dIII, *Kpn*I, *Xho*I and *Sal*I (Fig. 2B, b) and 1 μl of the Au–DNA particle in 100 μl final volume (3.5 nM final concentration for the endonucleases), as described in the Supplementary Information (Fig. S1), with only the modification of removing the reducing reagent from the reaction buffer and the enzymes in order to avoid detachment of the thiolated DNA from the gold nanoparticle.

REAL-TIME MEASUREMENT OF ENDONUCLEASE ACTIVITY, KINETICS AND INHIBITION

For kinetic measurements, *Xho*I was used as the model enzyme. The cleavage was also confirmed by FITC fluorescence images (see Supplementary Information, Fig. S3). The purpose of the FITC label removal experiment was solely for the validation of the enzymatic cleavage. The Au–DNA nanoconjugates were illuminated with a white light source for 20 min to completely photobleach the fluorescence prior to the spectroscopic measurement. The fluorescent label had no influence on the plasmon resonance measurement. The continuous acquisition of the scattering spectrum of a selected nanoparticle starts in synchronization with the introduction of the *Xho*I. For real-time kinetics measurement, one spectrum with 10 s integration time was acquired every minute. Significant blue shifts of the plasmon resonance wavelength were observed for the first 10 min and correlated with intensity decrease (Fig. 3B).

The rate of the endonuclease reaction on the Au–DNA nanoconjugate showed a concentration dependence, and was determined to followed a Michaelis–Menten enzyme kinetics[30] (Fig. 3B). The rate constants were 5.8×10^{-3} s^{-1} (3.5 nM) and 1.5×10^{-3} s^{-1} (350 pM). The inhibition of the endonuclease reactions on the Au–DNA nanoconjugates was achieved with the simultaneous addition of 10 mM EDTA and the 3.5-nM *Xho*I enzymes; the Mg^{2+} in the reaction buffer, which is required for *Xho*I activity, can be chelated by EDTA.

Bal-31 FOOTPRINTING OF *Eco*RI(Q111) BOUND ON dsDNA–Au

The cleavage-defective *Eco*RI(Q111) was purified according to previous descriptions[24–26], and incubated at 100 nM final concentration with the immobilized Au–DNA nanoconjugates (in this experiment, the FITC moiety was not used, so that exonuclease cleavage would not be affected) for 10 min in the 80 μl reaction buffer at 37 °C. Next, 20 μl *Bal*31 enzymes (Clontech) was added into the reaction buffer containing immobilized Au–DNA nanoconjugates in 100 μl final volume, with a *Bal*31 final concentration of 100 nM. The binding buffer contained 50 mM NaCl, 10 mM $MgCl_2$, 0.025% Triton X-100 and 100 mM Tris–HCl pH 7.5 at 25 °C.

Received 18 May 2006; accepted 29 August 2006; published 4 October 2006.

References

1. Behrens, S., Fuchs, B. M. & Amann, R. The effect of nucleobase-specific fluorescence quenching on in situ hybridization with rRNA-targeted oligonucleotide probes. *Syst. Appl. Microbiol.* **27,** 565–572 (2004).
2. Smith, J. & Anslyn, E. V. Radioactive end labeling to determine hydrolytic rates of nuclease mimics. *Anal. Biochem.* **220,** 53–57 (1994).
3. Hillier, S. C. *et al.* An electrochemical study of enzymatic oligonucleotide digestion. *Bioelectrochemistry* **63,** 307–310 (2004).

©2006 Nature Publishing Group

4. Alivisatos, A. P. *et al.* Organization of 'nanocrystal molecules' using DNA. *Nature* **382,** 609–611 (1996).
5. Zanchet, D., Micheel, C. M., Parak, W. J., Gerion, D. & Alivisatos, A. P. Electrophoretic isolation of discrete Au nanocrystal/DNA conjugates. *Nano Lett.* **1,** 32–35 (2001).
6. Taton, T. A., Mirkin, C. A. & Letsinger, R. L. Scanometric DNA array detection with nanoparticle probes. *Science* **289,** 1757–1760 (2000).
7. Storhoff, J. J., Elghanian, R., Mucic, R. C., Mirkin, C. A. & Letsinger, R. L. One-pot colorimetric differentiation of polynucleotides with single base imperfections using gold nanoparticle probes. *J. Am. Chem. Soc.* **120,** 1959–1964 (1998).
8. Mirkin, C. A., Letsinger, R. L., Mucic, R. C. & Storhoff, J. J. A DNA-based method for rationally assembling nanoparticles into macroscopic materials. *Nature* **382,** 607–609 (1996).
9. Sonnichsen, C., Reinhard, B. M., Liphardt, J. & Alivisatos, A. P. A molecular ruler based on plasmon coupling of single gold and silver nanoparticles. *Nature Biotechnol.* **23,** 741–745 (2005).
10. Homola, J., Yee, S. S. & Gauglitz, G. Surface plasmon resonance sensors: review. *Sensor Actuat. B-Chem.* **54,** 3–15 (1999).
11. Karlsson, R. SPR for molecular interaction analysis: a review of emerging application areas. *J. Mol. Recognit.* **17,** 151–161 (2004).
12. Mulvaney, P. Surface plasmon spectroscopy of nanosized metal particles. *Langmuir* **12,** 788–800 (1996).
13. Elghanian, R., Storhoff, J. J., Mucic, R. C., Letsinger, R. L. & Mirkin, C. A. Selective colorimetric detection of polynucleotides based on the distance-dependent optical properties of gold nanoparticles. *Science* **277,** 1078–1081 (1997).
14. Eck, D., Helm, C. A., Wagner, N. J. & Vaynberg, K. A. Plasmon resonance measurements of the adsorption and adsorption kinetics of a biopolymer onto gold nanocolloids. *Langmuir* **17,** 957–960 (2001).
15. Englebienne, P., Van Hoonacker, A. & Verhas, M. High-throughput screening using the surface plasmon resonance effect of colloidal gold nanoparticles. *Analyst* **126,** 1645–1651 (2001).
16. Nath, N. & Chilkoti, A. A colorimetric gold nanoparticle sensor to interrogate biomolecular interactions in real time on a surface. *Anal. Chem.* **74,** 504–509 (2002).
17. Sun, Y. G. & Xia, Y. N. Increased sensitivity of surface plasmon resonance of gold nanoshells compared to that of gold solid colloids in response to environmental changes. *Anal. Chem.* **74**, 5297–5305 (2002).
18. McFarland, A. D. & Van Duyne, R. P. Single silver nanoparticles as real-time optical sensors with zeptomole sensitivity. *Nano Lett.* **3,** 1057–1062 (2003).
19. Raschke, G. *et al.* Biomolecular recognition based on single gold nanoparticle light scattering. *Nano Lett.* **3,** 935–938 (2003).
20. Oldenburg, S. J., Genick, C. C., Clark, K. A. & Schultz, D. A. Base pair mismatch recognition using plasmon resonant particle labels. *Anal. Biochem.* **309,** 109–116 (2002).
21. Parak, W. J. *et al.* Conformation of oligonucleotides attached to gold nanocrystals probed by gel electrophoresis. *Nano Lett.* **3,** 33–36 (2003).
22. Bohren, C. F. & Huffman, D. R. *Absorption and Scattering of Light by Small Particles* (Wiley, New York, 1983).
23. Mazur, J. & Jernigan, R. L. Distance-dependent dielectric-constants and their application to double-helical DNA. *Biopolymers* **31,** 1615–1629 (1991).
24. King, K., Benkovic, S. J. & Modrich, P. Glu-111 is required for activation of the DNA cleavage center of EcoRI endonuclease. *J. Biol. Chem.* **264,** 11807–11815 (1989).
25. Pavco, P. A. & Steege, D. A. Elongation by *Escherichia coli* RNA polymerase is blocked in vitro by a site-specific DNA binding protein. *J. Biol. Chem.* **265,** 9960–9969 (1990).
26. Jett, S. D. & Bear, D. G. Snapshot blotting — Transfer of nucleic-acids and nucleoprotein complexes from electrophoresis gels to grids for electron-microscopy. *Proc. Natl Acad. Sci. USA* **91,** 6870–6874 (1994).
27. Legerski, R. J., Hodnett, J. L. & Gray, H. B.Jr. Extracellular nucleases of pseudomonas BAL 31. III. Use of the double-strand deoxyriboexonuclease activity as the basis of a convenient method for the mapping of fragments of DNA produced by cleavage with restriction enzymes. *Nucleic Acids Res.* **5,** 1445–1464 (1978).
28. Doron-Mor, I. *et al.* Sensitivity of transmission surface plasmon resonance (T-SPR) spectroscopy: Self-assembled multilayers on evaporated gold island films. *Chem. Eur. J.* **11,** 5555–5562 (2005).
29. Wanunu, M. *et al.* Branched coordination multilayers on gold. *J. Am. Chem. Soc.* **127,** 17877–17887 (2005).
30. Mizu, M., Koumoto, K., Kimura, T., Sakurai, K. & Shinkai, S. Protection of polynucleotides against nuclease-mediated hydrolysis by complexation with schizophyllan. *Biomaterials* **25,** 3109–3116 (2004).

Acknowledgements

This work was supported by DARPA, DOD BC045345, NIH R21CA95393, UCSF Prostate Cancer SPORE award (NIH P50 CA89520), and the UCSF Prostate Cancer Center Developmental Research Program, Intel, the Korea Ministry of Science and Technology "21st Century Frontier R&D Program" grant 05K1501-02810. This work was performed under the auspices of the U.S. Dept. of Energy, at the University of California/Lawrence Berkeley National Laboratory under contract no. DE-AC03-76SF00098 and at the University of California/Lawrence Livermore National Laboratory under contract no. W-7405-Eng-48.
Supplementary Information accompanies this paper on www.nature.com/naturenanotechnology.

Author contributions

F.F.C. conceived and designed the experiments, G.L.L., Y.Y., S.K. and B.M. performed the experiments, G.L.L. and D.G. analysed the data, and S.D.J. and D.G.B. synthesized the *Eco*RI(Q111).
Correspondence and requests for material should be addressed to F.F.C. and L.P.L.

Competing financial interests

The authors declare that they have no competing financial interests.

Reprints and permission information is available online at http://npg.nature.com/reprintsandpermissions/

©2006 Nature Publishing Group